PCCP

PAPER

Check for updates

Cite this: *Phys. Chem. Chem. Phys.*, 2017, **19**, 21112

Interaction of FeO^- with water: anion photoelectron spectroscopy and theoretical calculations†

Li-Juan Zhao,[ab] Xi-Ling Xu,*[a] Hong-Guang Xu,[a] Gang Feng[c] and Wei-Jun Zheng*[a]

Received 9th June 2017,
Accepted 14th July 2017

DOI: 10.1039/c7cp03870d

rsc.li/pccp

The interactions of FeO^- with water molecules were studied by using photoelectron spectroscopy and density functional theoretical calculations. It is found that a dihydroxyl species, $Fe(OH)_2^{-/0}$, can be formed when $FeO^{-/0}$ interacts with the first water molecule. The complexes formed *via* the interactions between $FeO^{-/0}$ and n water molecules can be viewed as $Fe(OH)_2(H_2O)_{n-1}^{-/0}$, in which $(n-1)H_2O$ molecules interact with a $Fe(OH)_2$ core. For $Fe(OH)_2^{-/0}$ and $Fe(OH)_2(H_2O)^-$, the $Fe(OH)_2$ unit has two conformers with the two OH groups oriented differently. The vertical detachment energies (VDEs) of $FeO_2H_2(H_2O)_{n-1}^-$ (n = 1–4) are measured to be 1.25 ± 0.04, 1.66 ± 0.04, 2.06 ± 0.04, and 2.37 ± 0.04 eV, respectively, by experiment. It is also worth mentioning that in the $FeO_2H_2(H_2O)^-$ anion the water molecule interacts with the $Fe(OH)_2$ core by forming a hydrogen bond with one of the OH groups, while in neutral $FeO_2H_2(H_2O)$, the water molecule interacts with the Fe atom of the $Fe(OH)_2$ core *via* its O atom.

I. Introduction

Iron plays an important role as an oxygen carrier in biological systems.[1] The corrosion of iron in humid air and water is very common in industry and our daily life.[2] Recently, iron oxides are regarded as good candidates as photocatalysts for solar water splitting because of their ideal band gap, chemical stability, non-toxicity, abundance, and low cost.[3,4] Investigation of the interaction between iron oxides and water is important for understanding the processes of oxygen transport in biological systems, corrosion of iron materials, and photocatalysis.

A large number of experimental and theoretical studies have been carried out on gaseous iron–oxygen–water systems during the past few decades.[5–16] Density functional theory (DFT) was used to study the $^{16}O/^{18}O$ exchange reactions of FeO^+ and $FeOH^+$ with $H_2{}^{18}O$ in the gas phase.[5] Fourier transform ion cyclotron resonance (FT-ICR) mass spectrometry experiments were conducted to investigate the reactions between FeO^+ and water as well as those of $Fe^+(H_2O)_n$ with O_2 and D_2O.[6–8] The pulsed photolysis/laser induced fluorescence technique and RRKM theory were employed to explore the FeO–H_2O reaction kinetics.[9] Thermochemistry of neutral and cationic iron hydroxides $Fe(OH)_n^{0/+}$ (n = 1, 2) in the gas phase was also investigated by mass spectrometry.[10] The bonding properties of cationic $FeOH_n^+$ (n = 0–2) were explored by DFT methods.[11] $Fe(OH)_2^+$ was predicted to be more stable than $(H_2O)FeO^+$ through combined electrospray ionization experiments and density functional theory calculations.[12] Low-energy collisionally activated dissociations (CAD) of $Fe[H_2, O_2]^+$ were also studied.[13] DFT studies on the interactions between water and small Fe_n clusters showed that $FeH_2O^{0/-}$ has an inserted HFeOH geometry while FeH_2O^+ has a water molecule interacting with the Fe atom.[17] The electronic and geometrical structures of $FeOH^{0/\pm}$ species were also investigated with DFT calculations.[18] In addition to the studies on neutral and singly charged species above, there were also a number of studies on doubly charged species. FT-ICR, sector field, and quadruple-based mass spectrometers as well as the B3LYP method were employed to explore the thermochemistry of $FeO_mH_n^{-/0/+/2+}$ (m = 1, 2; n = 0–4) species in the gas phase.[14] Charge-stripping mass spectrometry in conjunction with *ab initio* calculations was employed to probe the second ionization energies of gaseous iron oxides and hydroxides, $FeO_mH_n^{2+}$ (m = 1, 2; $n \leq 4$).[15] DFT study of high-valent iron(IV) dihydroxide $[Fe(OH)_2(H_2O)_4]^{2+}$ showed that $[Fe(OH)_2(H_2O)_4]^{2+}$ with a complete first hydration shell is easily converted into more stable iron(IV)-oxo species $[Fe(O)(H_2O)_5]^{2+}$.[16]

In this work, we conducted a combined anion photoelectron spectroscopy and theoretical study on $FeO_2H_2(H_2O)_{n-1}^-$ (n = 1–4)

[a] *Beijing National Laboratory for Molecular Sciences, State Key Laboratory of Molecular Reaction Dynamics, Institute of Chemistry, Chinese Academy of Sciences, Beijing 100190, China. E-mail: xlxu@iccas.ac.cn, zhengwj@iccas.ac.cn; Fax: +86 10 62563167; Tel: +86 10 62635054*

[b] *University of Chinese Academy of Sciences, Beijing 100049, China*

[c] *School of Chemistry and Chemical Engineering, Chongqing University, Chongqing 401331, China*

† Electronic supplementary information (ESI) available. See DOI: 10.1039/c7cp03870d

This journal is © the Owner Societies 2017

clusters in order to understand the interactions between iron oxide and water molecules in the gas phase.

II. Experimental and theoretical methods

A. Experimental methods

The experiments were carried out on a home-built apparatus, which consists of a linear time-of-flight (TOF) mass spectrometer and a magnetic-bottle photoelectron spectrometer.[19] The FeO^- and $FeO_2H_2(H_2O)_{n-1}^-$ (n = 1–4) anions were produced by using a laser vaporization source. The second harmonic (532 nm) light pulses of a Nd:YAG laser (Continuum Surelite II-10) ablated a rotating and translating Fe disc target. The residual oxygen on the target surface is enough for generating iron oxide. The typical laser power used for vaporization was about 10 mJ per pulse in this work. Helium carrier gas with ~4 atm backing pressure seeded with water vapor was allowed to expand through a pulsed valve (General Valve Series 9) over the target. The reaction of iron oxide with water molecules generated the resultant cluster anions. The FeO^- and $FeO_2H_2(H_2O)_{n-1}^-$ (n = 1–4) anions were selected using a mass gate, decelerated by a momentum decelerator, and photodetached with the beam of another Nd:YAG laser (Continuum Surelite II-10; 355 and 266 nm). The photoelectrons produced were energy-analyzed using the magnetic-bottle photoelectron spectrometer. The photoelectron spectra were calibrated using the spectra of Cu^- and Au^- obtained under similar conditions. The resolution of the photoelectron spectrometer was about 40 meV for electrons with 1 eV kinetic energy.

B. Computational methods

Theoretical calculations of FeO^- and $FeO_2H_2(H_2O)_{n-1}^-$ (n = 1–4) and their neutrals were conducted using density functional theory with the B3LYP[20–22] method and the 6-311+G(d,p) basis set. The geometric optimizations were conducted with numerous possible initial geometries at doublet, quartet, sextet, and octet spin multiplicities for the anions and at singlet, triplet, quintet, and septet spin multiplicities for their neutrals. No symmetry constraints were imposed during the optimizations. Harmonic vibrational frequencies were also analyzed at the same level to verify that the obtained structures are true local minima on the potential energy surfaces. The single-point energies were then calculated with the B3LYP method and the augmented correlation-consistent polarized valence triple-zeta basis sets (aug-cc-pVTZ).[23] The vertical detachment energies (VDEs) of the anions were calculated as the energy differences between the neutrals and anions with both neutrals and anions at the equilibrium structures of the anions, whereas the adiabatic detachment energies (ADEs) of the anions were calculated as the energy differences between the neutrals and the anions with the neutrals relaxed to the nearest local minima using the anionic structures as initial structures. The hydrogen bonds formed were also analyzed to investigate the interaction between the $Fe(OH)_2$ unit and water molecules. Analyses of canonical molecular orbitals (CMOs) were performed to understand their bonding properties. All the calculations were performed using the Gaussian 09 program package.[24]

III. Experimental and theoretical results

The photoelectron spectra of FeO^- and $FeO_2H_2(H_2O)_{n-1}^-$ (n = 1–4) taken with 355 nm and 266 nm photons are presented in Fig. 1 and 2, respectively. The typical low-lying isomers of $FeO_2H_2(H_2O)_{n-1}^-$ (n = 1–4) are shown in Fig. 3, and those of their corresponding neutrals are shown in Fig. 4. More low-lying isomers of $FeO_2H_2(H_2O)_{n-1}^-$ and $FeO_2H_2(H_2O)_{n-1}$ (n = 1–4) can be found in Fig. S1 and S2 of the ESI.† The theoretical ADEs and VDEs of the typical isomers of FeO^- and $FeO_2H_2(H_2O)_{n-1}^-$ (n = 1–4) calculated at the B3LYP level of theory are listed in Table 1 (and Table S1 in the ESI†) along with the experimental ones for comparison. From Table 1 and Table S1 (ESI†), we can see that the theoretical ADE/VDE values of FeO^- are 1.48/1.50 eV at the B3LYP/6-311+G(d,p) level and 1.47/1.49 eV at the B3LYP/aug-cc-pVTZ level, which are in good agreement with the experimental ones (1.52/1.52 eV). The structural and electronic properties of FeO and FeO^- were investigated previously with BPW91,

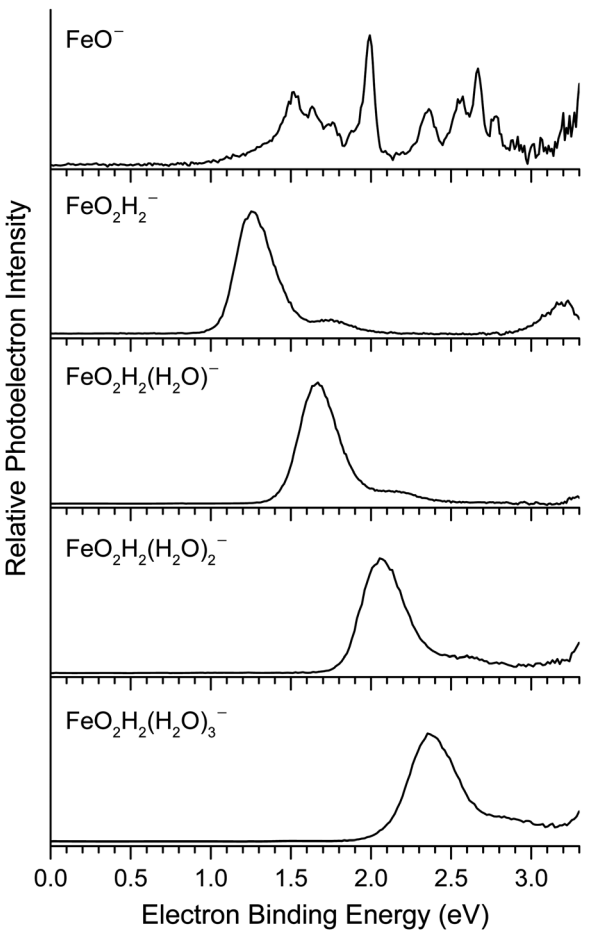

Fig. 1 Photoelectron spectra of FeO^- and $FeO_2H_2(H_2O)_{n-1}^-$ (n = 1–4) taken with 355 nm photons.

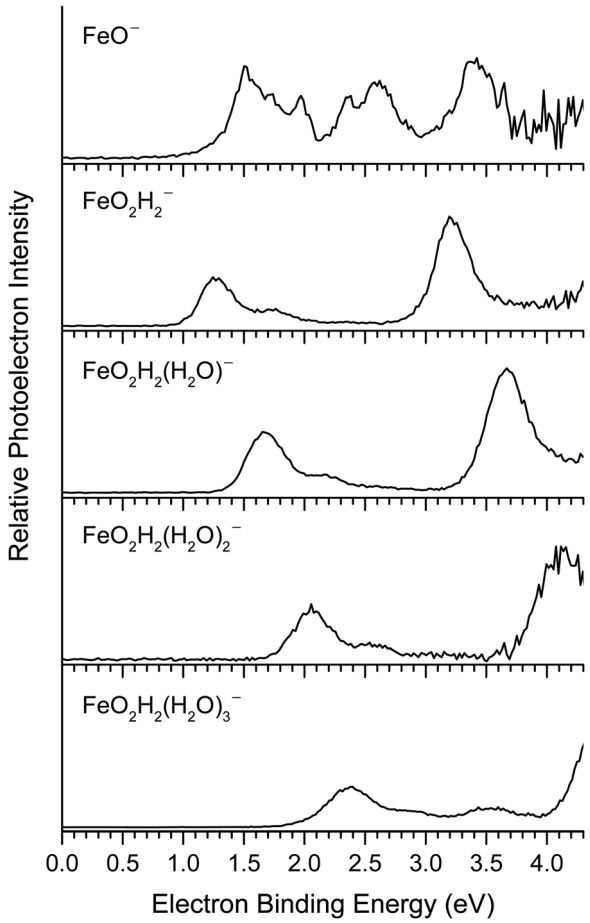

Fig. 2 Photoelectron spectra of FeO^- and $FeO_2H_2(H_2O)_{n-1}^-$ (n = 1–4) taken with 266 nm photons.

BLYP, and B3LYP density functionals,[25] indicating that the B3LYP method and 6-311+G(d,p) and aug-cc-pVTZ basis sets can be applied to the iron–oxygen–water system. As the theoretical VDEs at the B3LYP/aug-cc-pVTZ level are closer to the experimental ones than those at the B3LYP/6-311+G(d,p) level, the theoretical VDEs discussed in the theoretical results part are from the B3LYP/aug-cc-pVTZ level.

A. Experimental results

As seen in Fig. 1, four bands are observed for FeO^- at 1.50–1.90, 1.99, 2.36, and 2.50–3.00 eV, in which the first and fourth bands are vibrationally resolved. The band between 1.50 and 1.90 eV is resolved into four vibrational peaks centered at 1.52, 1.63, 1.75, and 1.88 eV. The band between 2.50 and 3.00 eV is resolved into four vibrational peaks centered at 2.56, 2.66, 2.77, and 2.89 eV. The tail in the range of 1.1–1.5 eV is assigned to be a hot band, resulting from the vibrational excited FeO^- anion. From the first peak in the 355 nm spectrum, the experimental ADE/VDE value of FeO^- is determined to be 1.52/1.52 eV and the VDE value is in agreement with the previous experimental value (1.50 eV).[26]

Unlike FeO^-, the 266 nm spectrum of $FeO_2H_2^-$ in Fig. 2 has two dominant broad features centered at 1.25 and 3.22 eV, and a shoulder in the range of 1.60–2.00 eV. Due to the low detection efficiency of the slow electrons, the peak at 3.22 eV becomes weaker in the 355 nm spectrum than that in the 266 nm spectrum. The spectrum of $FeO_2H_2^-$ is not similar to that of FeO^-, indicating that $FeO_2H_2^-$ cannot be simply regarded as $FeO(H_2O)^-$ (simple hydration of FeO^-).

Interestingly, the photoelectron spectra of $FeO_2H_2(H_2O)_{n-1}^-$ (n = 2–4) are similar to that of $FeO_2H_2^-$, that is, they all have two major bands and an additional shoulder following the first one. Their spectral features shift toward higher electron binding energy with increasing number of water molecules. These similarities suggest that the additional water molecules have simple solvent effects on the $FeO_2H_2^-$ cluster. The spectral peaks of $FeO_2H_2(H_2O)_3^-$ shift toward higher electron binding energy; thus, only the onset of its third band is observed in the 266 nm spectrum. It is worth mentioning that the peak in the range of 3.0–4.0 eV in the 266 nm spectrum of $FeO_2H_2(H_2O)_3^-$ may come from impurities.

B. Theoretical results

The most stable isomers of $FeO_2H_2^-$ (**1A** and **1B**) are C_2 symmetry dihydroxyl species in the form of $Fe(OH)_2^-$ with the two OH groups oriented differently. The theoretical ADE/VDE values of **1A** and **1B** are calculated to be 1.18/1.31 eV, in good agreement with the experimental ADE/VDE values (1.10/1.25 eV). Isomers **1C** and **1D** are much higher in energy than **1A** and **1B**. **1C** has an OH group, an O atom, and an H atom bonded to the central Fe atom. **1D** is a hydrated iron oxide species with one water molecule absorbed on the O atom side *via* one hydrogen bond, which can be written as $FeO^-\cdot(H_2O)$. The theoretical VDEs of **1C** and **1D** are much higher than the experimental VDE of $FeO_2H_2^-$. So it is unlikely for **1C** and **1D** to be present in our experiments. Isomers **1A** and **1B** are the most probable isomers contributing to the photoelectron spectra of $FeO_2H_2^-$. Similar to $FeO_2H_2^-$, the most stable structures of FeO_2H_2, **1a** and **1b**, are also dihydroxyl species in the form of $Fe(OH)_2$. The $(H_2O)FeO$ type of structure (**1c**) is higher in energy than the dihydroxyl structure by 2.17 eV.

The most stable isomers of $FeO_2H_2(H_2O)^-$ (**2A** and **2B**) are derived from those of $Fe(OH)_2^-$ with the O atom of the $Fe(OH)_2$ unit interacting with the water molecule *via* one hydrogen bond. The calculated ADE/VDE values of **2A** and **2B** are 1.27/1.78 and 1.27/1.77 eV, in good agreement with the experimental ones (1.48/1.66 eV). Isomers **2C** and **2D** are much higher in energy than **2A** and **2B**. Their theoretical VDEs are also much higher than the experimental VDE of $FeO_2H_2(H_2O)^-$. Therefore, the existence of **2C** and **2D** in the experiments can be ruled out. Isomers **2A** and **2B** are the most probable ones contributing to the photoelectron spectra of $FeO_2H_2(H_2O)^-$. Different from the structure of the $FeO_2H_2(H_2O)^-$ anion, the most stable structure of neutral $FeO_2H_2(H_2O)$ (**2a**) has a water molecule interacting with the $Fe(OH)_2$ unit through a Fe···O bond.

The most stable isomer of $FeO_2H_2(H_2O)_2^-$ (**3A**) is in the form of $Fe(OH)_2(H_2O)_2^-$ with two water molecules interacting with the two OH groups of the $Fe(OH)_2$ unit *via* two hydrogen bonds. The theoretical VDE value of **3A** (2.21 eV) is in good agreement with the experimental VDE (2.06 eV). Isomers **3B** and **3C** are also in the form of $Fe(OH)_2(H_2O)_2^-$, but with two water molecules

 This journal is © the Owner Societies 2017

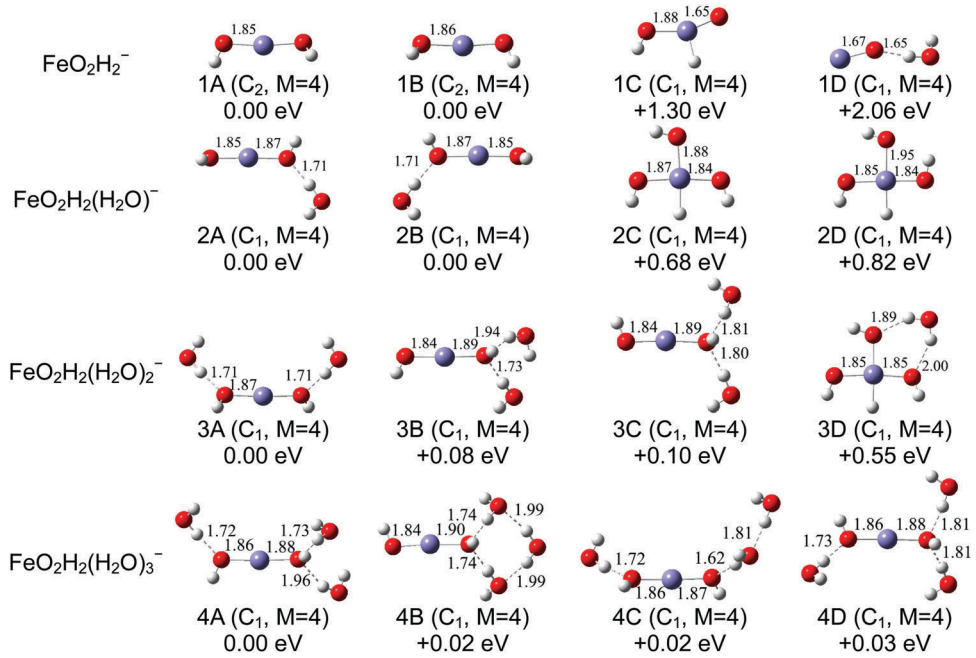

Fig. 3 Typical low-lying isomers of $FeO_2H_2(H_2O)_{n-1}^-$ (n = 1–4) clusters. The O···H and Fe–O bond distances (in Å) are labeled. The symmetries and spin multiplicities (M for short) are shown under the structures. Their relative energies (in eV) with respect to the most stable isomers at the B3LYP/aug-cc-pVTZ level are listed.

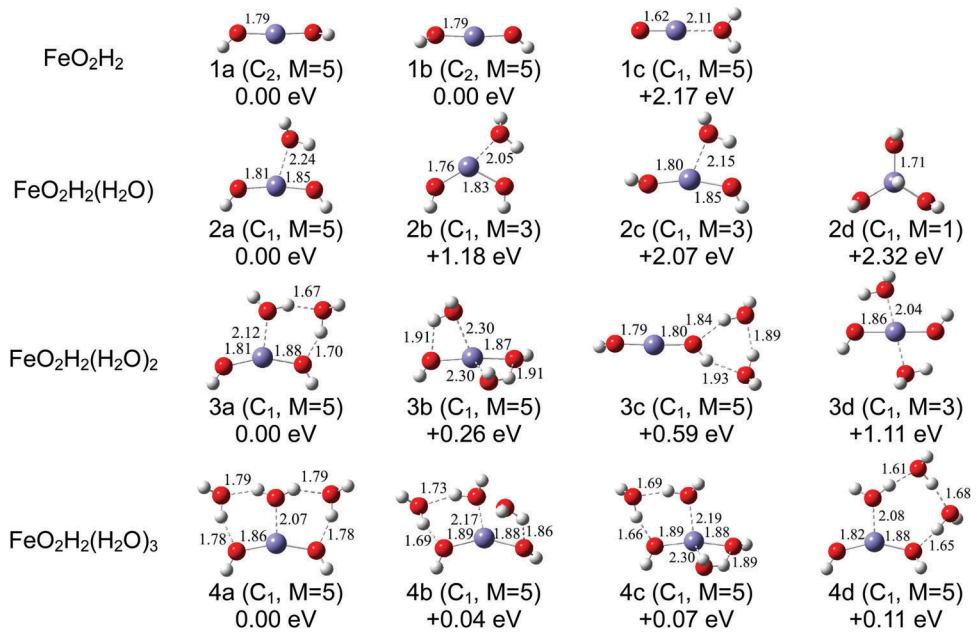

Fig. 4 Typical low-lying isomers of $FeO_2H_2(H_2O)_{n-1}$ (n = 1–4) clusters. The O···H and Fe–O bond distances (in Å) are labeled. The symmetries and spin multiplicities (M for short) are shown under the structures. Their relative energies (in eV) with respect to the most stable isomers at the B3LYP/aug-cc-pVTZ level are listed.

interacting with one OH group of the $Fe(OH)_2$ unit *via* hydrogen bonds. The energies of **3B** and **3C** are higher than that of **3A** by 0.08 and 0.10 eV. Their VDEs (2.13 and 2.21 eV) are also in good agreement with the experimental VDE. Isomer **3D** is less stable than isomer **3A** by 0.55 eV. The calculated VDE of **3D** is 3.59 eV, which is much larger than the experimental one. The existence of **3D** in the experiments can be ruled out. Thus, we suggest that isomers **3A**, **3B**, and **3C** contributed to the experimental spectra of $FeO_2H_2(H_2O)_2^-$. For neutral $FeO_2H_2(H_2O)_2$, the most stable isomer **3a** is also in the form of $Fe(OH)_2(H_2O)_2$ in which one H_2O interacts with the Fe atom of the $Fe(OH)_2$ core *via* a Fe···O bond while the other H_2O interacts with the O atom of

Table 1 Relative energies, ADEs and VDEs (in eV) of the typical low-lying isomers of FeO^- and $FeO_2H_2(H_2O)_{n-1}^-$ (n = 1–4) clusters calculated at the B3LYP level, as compared to the experimental ADEs and VDEs

			ADE[b] (eV)		VDE (eV)	
Isomer		ΔE^a (eV)	Theo.[a]	Expt.	Theo.[a]	Expt.
FeO^-		0.00	1.47	1.52 ± 0.04	1.49	1.52 ± 0.04
$FeO_2H_2^-$	1A	0.00	1.18	1.10 ± 0.04	1.31	1.25 ± 0.04
	1B	0.00	1.18		1.31	
	1C	1.30	2.60		2.76	
	1D	2.06	1.28		1.98	
$FeO_2H_2(H_2O)^-$	2A	0.00	1.27	1.48 ± 0.04	1.78	1.66 ± 0.04
	2B	0.00	1.27		1.77	
	2C	0.68	2.51		3.02	
	2D	0.82	2.32		3.09	
$FeO_2H_2(H_2O)_2^-$	3A	0.00	1.43	1.85 ± 0.04	2.21	2.06 ± 0.04
	3B	0.08	1.10		2.13	
	3C	0.10	1.15		2.21	
	3D	0.55	3.05		3.59	
$FeO_2H_2(H_2O)_3^-$	4A	0.00	1.27	2.11 ± 0.04	2.55	2.37 ± 0.04
	4B	0.02	2.01		2.46	
	4C	0.02	1.25		2.48	
	4D	0.03	1.27		2.65	

[a] Calculated at the B3LYP/aug-cc-pVTZ//B3LYP/6-311+G(d,p) level. [b] As the experimental ADEs may not represent the real ADEs in some cases due to the large geometric differences between anions and neutrals, we mainly discuss the VDEs.

the $Fe(OH)_2$ core *via* a hydrogen bond. A H–O···Fe–O···H–O six-membered ring is formed by the two water molecules and the $Fe(OH)_2$ unit. The arrangement of the water molecules in neutral $FeO_2H_2(H_2O)_2$ is different from that in the $FeO_2H_2(H_2O)_2^-$ anion.

The most stable isomer of $FeO_2H_2(H_2O)_3^-$ (**4A**) is in the form of $Fe(OH)_2(H_2O)_3^-$ with three water molecules interacting with the $Fe(OH)_2$ unit *via* three hydrogen bonds. The VDE value of **4A** is calculated to be 2.55 eV, in reasonable agreement with the experimental one (2.37 eV). Isomers **4B**, **4C**, and **4D** are also in the form of $Fe(OH)_2(H_2O)_3^-$, which are less stable than **4A** by 0.02, 0.02, and 0.03 eV in energy, respectively. The calculated VDEs of **4B**, **4C**, and **4D** are 2.46, 2.48, and 2.65 eV, respectively. The geometric differences among isomers **4A**, **4B**, **4C**, and **4D** are very small because they are all formed from a $Fe(OH)_2$ core and three water molecules. Isomers **4A**, **4B**, **4C**, and **4D** may all contribute to the experimental spectra of $FeO_2H_2(H_2O)_3^-$ because the experimental feature is fairly broad extending from 2.1 to 2.7 eV. For neutral $FeO_2H_2(H_2O)_3$, the structure is different from the anion; the most stable isomer (**4a**) is in the form of $Fe(OH)_2(H_2O)_3$ with one H_2O interacting with the Fe atom of $Fe(OH)_2$ *via* a Fe···O bond and the other two H_2O molecules interacting correspondingly with the two O atoms of $Fe(OH)_2$ *via* a hydrogen bond. The three water molecules and the $Fe(OH)_2$ unit form two co-edge H–O···Fe–O···H–O six-membered rings.

Overall, the structures of $FeO_2H_2(H_2O)_{n-1}^-$ and $FeO_2H_2(H_2O)_{n-1}$ (n = 2–4) can be viewed as n water molecules interacting with a $Fe(OH)_2$ core. The difference between the structures of the anionic and neutral species is that, in the anionic species, the water molecules interact with the O atoms of the $Fe(OH)_2$ core *via* O···H–O hydrogen bonds, while in the neutral species, one of the water molecules connects to the Fe atom of the $Fe(OH)_2$ core through its O atom.

In order to investigate the interaction between the $Fe(OH)_2$ unit and the water molecules, we analyzed the hydrogen bonds

Table 2 Analyses of the hydrogen bonds in $FeO_2H_2(H_2O)_{n-1}^-$ (n = 2–4)

	Isomer	Bond	d_{O-H} (Å)	ν(O–H) (cm^{-1})	$d_{O\cdots H}$ (Å)	Δd (Å)	ΔE (kcal mol^{-1})
H_2O		O–H	0.96	3817(s); 3923(a)			
$FeO_2H_2(H_2O)^-$	2A	O3···H8–O6	1.00	3232	1.71	−0.89	−14.6
	2B	O3···H7–O6	1.00	3234	1.71	−0.89	−14.6
$FeO_2H_2(H_2O)_2^-$	3A	O2···H11–O9	0.99	3270(s); 3260(a)	1.71	−0.89	−14.2
		O3···H8–O6	0.99		1.71		
	3B	O2···H7–O6	0.99	3585(s); 3262(a)	1.73	−0.77	−13.3
		O2···H10–O9	0.98		1.94		
	3C	O3···H7–O6	0.99	3421(s); 3382(a)	1.81	−0.80	−13.0
		O3···H10–O9	0.99		1.80		
$FeO_2H_2(H_2O)_3^-$	4A	O2···H7–O6	0.99	3287(a); 3299(a); 3608(s)	1.72	−0.80	−13.2
		O3···H11–O9	0.99		1.73		
		O3···H13–O12	0.98		1.96		
	4B	O3···H7–O6	0.99	3273(a); 3336(s); 3660(a)3705(a);	1.74	−0.74	−9.8
		O3···H10–O9	0.99		1.74		
		O6···H14–O12	0.97		1.99		
		O9···H13–O12	0.97		1.99		
	4C	O3···H8–O6	0.99	3007(a); 3289(s); 3488(a)	1.72	−0.88	−13.1
		O2···H11–O9	1.01		1.62		
		O9···H13–O12	0.98		1.81		
	4D	O2···H11–O9	0.99	3445(s); 3411(a); 3304(a)	1.81	−0.82	−13.0
		O2···H13–O12	0.99		1.81		
		O3···H8–O6	0.99		1.73		

d_{O-H}: O–H bond lengths. $d_{O\cdots H}$: O···H distances in hydrogen bonds. ν(O–H): O–H stretching vibrational frequency of the O–H bonds. Δd: difference between the O···H distance and the sum of the van der Waals radii of O and H.ΔE: interaction energy per hydrogen bond calculated at the B3LYP/aug-cc-pVTZ level. s: symmetric stretching vibration mode. a: asymmetric stretching vibration mode.

 This journal is © the Owner Societies 2017

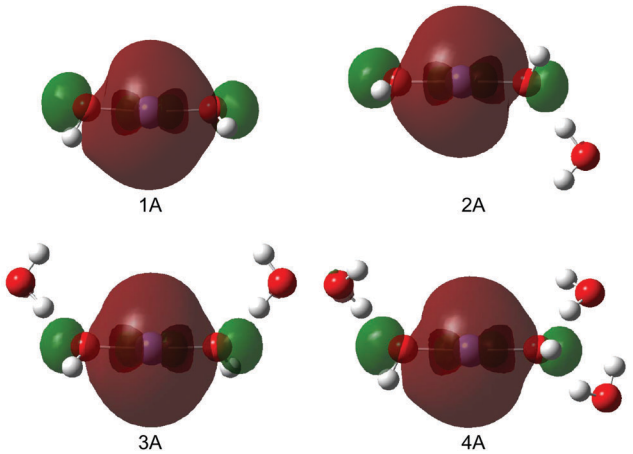

Fig. 5 Highest occupied molecular orbitals (HOMOs) of the most stable isomers of $FeO_2H_2(H_2O)_{n-1}^-$ (n = 1–4).

(O···H–O) in $FeO_2H_2(H_2O)_{n-1}^-$ (n = 2–4). From the negative Δd values in Table 2, it can be concluded that the O···H distances are smaller than 2.60 Å, the sum of the van der Waals radii of O atom (1.40 Å) and H atom (1.20 Å).[27] It can be seen in Table 2 that the O–H bond length (d_{O-H}) of $FeO_2H_2(H_2O)_{n-1}^-$ (n = 2–4) is in the range of 0.97–1.01 Å, larger than that in H_2O (0.96 Å). The O–H stretching vibrational frequencies, ν(O–H), of $FeO_2H_2(H_2O)_{n-1}^-$ are lower than those of H_2O (3817 cm^{-1} for ν_s and 3923 cm^{-1} for ν_a). These results indicate that the formation of hydrogen bonds weakens the O–H bonds and causes the O–H stretching vibrational frequencies to shift toward the infrared region. It can also be seen that the absolute value of the interaction energy per hydrogen bond (ΔE) decreases slightly with increasing number of water molecules and hydrogen bonds. We have also calculated the successive binding energies of H_2O for these species. The successive binding energies of H_2O for the most stable structures of $FeO_2H_2(H_2O)^-$ (**2A**), $FeO_2H_2(H_2O)_2^-$ (**3A**), and $FeO_2H_2(H_2O)_3^-$ (**4A**) are calculated to be −14.6, −13.8, and −13.1 kcal mol^{-1}, respectively, indicating that the interaction between the $Fe(OH)_2$ core and H_2O becomes slightly weaker with increasing number of water molecules which agrees with the results of the interaction energy per hydrogen bond.

The highest occupied molecular orbitals (HOMOs) of $FeO_2H_2(H_2O)_{n-1}^-$ (n = 1–4) are analyzed and are shown in Fig. 5 (and Fig. S3 in the ESI†). The HOMO of $FeO_2H_2^-$ is mainly composed of 3d and 4s atomic orbitals of the Fe atom and the 2p atomic orbitals of the two O atoms. Similar to the HOMO of $FeO_2H_2^-$, the HOMOs of $FeO_2H_2(H_2O)_{n-1}^-$ (n = 2–4) are also mainly composed of the 3d and 4s atomic orbitals of the Fe atom and the 2p atomic orbitals of the two O atoms connecting to the Fe atom. Therefore, their HOMOs mainly localize on the $Fe(OH)_2$ core. This indicates that the first spectral features in the photoelectron spectra of $FeO_2H_2(H_2O)_{n-1}^-$ (n = 1–4) come from the detachment of one electron from the $Fe(OH)_2$ core, which is in agreement with the observation in the experiment that the photoelectron spectral features of $FeO_2H_2(H_2O)_{1-3}^-$ are similar to those of $FeO_2H_2^-$ but shift toward higher electron binding energy due to the solvation effects of water molecules.

IV. Conclusions

The interactions of FeO^- with water molecules were explored with photoelectron spectroscopy and density functional theoretical calculations. The vertical detachment energies (VDEs) of $FeO_2H_2(H_2O)_{n-1}^-$ (n = 1–4) were measured to be 1.25 ± 0.04, 1.66 ± 0.04, 2.06 ± 0.04, and 2.37 ± 0.04 eV, respectively, by experiment. The possible structures of $FeO_2H_2(H_2O)_{n-1}^-$ (n = 1–4) were determined by comparison of theoretical calculations with experimental results. When $FeO^{-/0}$ interacts with the first water molecule, a dihydroxyl species, $Fe(OH)_2^{-/0}$, was formed. The structures of $FeO_2H_2(H_2O)_{n-1}^-$ and $FeO_2H_2(H_2O)_{n-1}$ (n = 2–4) can be viewed as n water molecules interacting with a $Fe(OH)_2$ core. In $FeO_2H_2(H_2O)^-$, the water molecule interacts with the $Fe(OH)_2$ core by forming a hydrogen bond with one of the OH groups, while in neutral $FeO_2H_2(H_2O)$, the water molecule interacts with the Fe atom of the $Fe(OH)_2$ core *via* its O atom. The HOMOs of $FeO_2H_2(H_2O)_{n-1}^-$ (n = 1–4) mainly localize on the Fe atom and two O atoms of the $Fe(OH)_2$ units.

Conflicts of interest

There are no conflicts of interest to declare.

Acknowledgements

This work was supported by the National Natural Science Foundation of China (Grant No. 21543007 and 21403249) and the Chinese Academy of Sciences (Grant No. QYZDB-SSW-SLH024). The theoretical calculations were performed on the Scientific Computing Grid (ScGrid) of the Supercomputing Center, Computer Network Information Center of the Chinese Academy of Sciences.

References

1 H. Chen, M. Ikeda-Saito and S. Shaik, *J. Am. Chem. Soc.*, 2008, **130**, 14778–14790.
2 A. M. Mebel and D.-Y. Hwang, *J. Phys. Chem. A*, 2001, **105**, 7460–7467.
3 Y. Lin, G. Yuan, S. Sheehan, S. Zhou and D. Wang, *Energy Environ. Sci.*, 2011, **4**, 4862–4869.
4 I. Cesar, A. Kay, J. A. Gonzalez Martinez and M. Grätzel, *J. Am. Chem. Soc.*, 2006, **128**, 4582–4583.
5 S. Bärsch, D. Schröder and H. Schwarz, *Chem. – Eur. J.*, 2000, **6**, 1789–1796.
6 M. Brönstrup, D. Schröder and H. Schwarz, *Chem. – Eur. J.*, 1999, **5**, 1176–1185.
7 C. van der Linde, S. Hemmann, R. F. Höckendorf, O. P. Balaj and M. K. Beyer, *J. Phys. Chem. A*, 2013, **117**, 1011–1020.
8 C. van der Linde and M. K. Beyer, *J. Phys. Chem. A*, 2012, **116**, 10676–10682.
9 R. J. Rollason and J. M. C. Plane, *Phys. Chem. Chem. Phys.*, 2000, **2**, 2335–2343.
10 D. Schröder and H. Schwarz, *Int. J. Mass Spectrom.*, 2003, **227**, 121–134.
11 X. Zhang and H. Schwarz, *Theor. Chem. Acc.*, 2011, **129**, 389–399.

12 D. Schröder, S. O. Souvi and E. Alikhani, *Chem. Phys. Lett.*, 2009, **470**, 162–165.
13 D. Vukomanovic and J. A. Stone, *Int. J. Mass Spectrom.*, 2000, **202**, 251–259.
14 D. Schröder, *J. Phys. Chem. A*, 2008, **112**, 13215–13224.
15 D. Schröder, S. Bärsch and H. Schwarz, *J. Phys. Chem. A*, 2000, **104**, 5101–5110.
16 F. Buda, B. Ensing, M. C. M. Gribnau and E. J. Baerends, *Chem. – Eur. J.*, 2001, **7**, 2775–2783.
17 G. L. Gutsev, M. D. Mochena and C. W. Bauschlicher Jr, *Chem. Phys.*, 2005, **314**, 291–298.
18 G. L. Gutsev, M. D. Mochena and C. W. Bauschlicher Jr, *Chem. Phys. Lett.*, 2005, **407**, 180–185.
19 H.-G. Xu, Z.-G. Zhang, Y. Feng, J. Yuan, Y. Zhao and W. Zheng, *Chem. Phys. Lett.*, 2010, **487**, 204–208.
20 A. D. Becke, *Phys. Rev. A: At., Mol., Opt. Phys.*, 1988, **38**, 3098–3100.
21 A. D. Becke, *J. Chem. Phys.*, 1993, **98**, 5648–5652.
22 C. Lee, W. Yang and R. G. Parr, *Phys. Rev. B: Condens. Matter Mater. Phys.*, 1988, **37**, 785–789.
23 R. A. Kendall, T. H. Dunning and R. J. Harrison, *J. Chem. Phys.*, 1992, **96**, 6796–6806.
24 M. J. Frisch, G. W. Trucks, H. B. Schlegel, G. E. Scuseria, M. A. Robb, J. R. Cheeseman, G. Scalmani, V. Barone, B. Mennucci, G. A. Petersson, H. Nakatsuji, M. Caricato, X. Li, H. P. Hratchian, A. F. Izmaylov, J. Bloino, G. Zheng, J. L. Sonnenberg, M. Hada, M. Ehara, K. Toyota, R. Fukuda, J. Hasegawa, M. Ishida, T. Nakajima, Y. Honda, O. Kitao, H. Nakai, T. Vreven, J. A. Montgomery Jr., J. E. Peralta, F. Ogliaro, M. J. Bearpark, J. Heyd, E. N. Brothers, K. N. Kudin, V. N. Staroverov, R. Kobayashi, J. Normand, K. Raghavachari, A. P. Rendell, J. C. Burant, S. S. Iyengar, J. Tomasi, M. Cossi, N. Rega, N. J. Millam, M. Klene, J. E. Knox, J. B. Cross, V. Bakken, C. Adamo, J. Jaramillo, R. Gomperts, R. E. Stratmann, O. Yazyev, A. J. Austin, R. Cammi, C. Pomelli, J. W. Ochterski, R. L. Martin, K. Morokuma, V. G. Zakrzewski, G. A. Voth, P. Salvador, J. J. Dannenberg, S. Dapprich, A. D. Daniels, Ö. Farkas, J. B. Foresman, J. V. Ortiz, J. Cioslowski and D. J. Fox, *Gaussian 09, revision D.01*, Gaussian, Inc., Wallingford, CT, USA, 2009.
25 G. L. Gutsev, B. K. Rao and P. Jena, *J. Phys. Chem. A*, 2000, **104**, 5374–5379.
26 J. Fan and L. S. Wang, *J. Chem. Phys.*, 1995, **102**, 8714–8717.
27 L. Pauling, *The Nature of the Chemical Bond*, Cornell University Press, New York, 3rd edn, 1960.

 This journal is © the Owner Societies 2017